Exploring the Impact of TiO₂ and MgO Nanoparticles on the Mechanical and Topographical Characteristics of Glass Fiber Reinforced Polymer (GFRP) Composites with Varied Lay-up Sequences: A Taguchi Analysis

A. Somaiah [a, *], B. Anjaneya Prasad [a], N. Kishore Nath [b]

[a] Department of Mechanical Engineering, J.N.T. University, Kukatpally, Hyderabad-500085, India

[b] Advanced Systems Laboratory, DRDO, Kanchanbagh, Hyderabad-500058, India

*Corresponding Author Email: anabathula.somaiah@gmail.com

Abstract: A revolutionary composite material, blending Glass Fiber Reinforced Polymer (GFRP) with advanced nanofillers like TiO₂ and MgO, showcases remarkable versatility in various industries due to its unique properties. The process involves precise control of key factors, including fiber stacking sequence (F.S.S) and nanofiller integration (MgO and TiO₂). The vacuum bagging process is employed in the production of nanocomposite laminates. Experimental studies have been conducted to assess the performance of composites with and without nanofillers, with a specific focus on crucial mechanical properties, namely ultimate tensile strength (U.T.S), flexural strength (F.S), impact strength (I.S), and hardness (H). The Taguchi L9 orthogonal array design optimizes parameters and enhances mechanical properties. Comparisons reveal significant improvements with nanofillers, including a 31.96% increase in ultimate tensile strength and a substantial 68.43% enhancement in flexural strength. ANOVA results highlight the critical impact of fiber stacking sequence on ultimate tensile strength (63.65%), flexural strength (65.70%), and impact strength (9.30%), while nanofillers play a lesser role, contributing 11.71% to ultimate tensile strength, 2.66% to flexural strength, and 3.61% to impact strength. Notably, in composite hardness, nanofillers play a more significant role, contributing 39.22%, while the influence of fiber stacking sequence is lower at 3.29%.

Keywords: TiO₂, MgO, Taguchi's Approach, ANOVA, Stacking sequence

1. Introduction

A composite combines two elements, typically a continuous matrix and discontinuous reinforcement. Glass fiber-reinforced polymer composites are renowned for their lightweight, corrosion resistance, high strength, excellent mechanical properties, low thermal expansion, and durability. Utilizing Nano fillers offers the advantage of needing fewer fillers to achieve specific multifunctional properties, compared to traditional micro-scale fillers. Combining GFRP composites with Nano fillers significantly enhances their performance, particularly in structural applications [1]. Different production parameter combinations yield distinct optimal outcomes. The primary determinant seems to be the drying temperature of bamboo fibers. Elevated temperatures may degrade properties and the bonding interface with the epoxy matrix. Conversely, shorter drying durations, fiber lengths, and a lower bamboo-to-glass fiber ratio positively impact composite properties [2]. Titanium dioxide (TiO₂) is a versatile filler material gaining attention for its extensive applications.

Additionally, TiO₂ serves as an effective UV-resistant material due to its chemical inertness, non-toxic nature, affordability, high refractive index, and advantageous surface characteristics [3]. In the production of glass/epoxy composites, four layers of unidirectional E-glass fibers are integrated and enhanced with nanoparticles like multiwall carbon nanotubes, nano-iron oxide, and nano-silica. It's noteworthy that, across all specimen types, the ultimate tensile strength declines with increasing nanoparticle quantity due to their tendency to aggregate, impacting mechanical properties and interfacial adhesion. While nano-fillers improve properties initially, their aggregation, driven by VanderWaals forces, causes composite properties to deteriorate, influenced by filler geometry and concentration [4, 5]. In GFRP burning characteristics, adding pumice and reducing aluminum trihydroxide quantity notably prolonged ignition time and lowered the burning rate. Higher pumice concentration significantly enhanced flexural and impact strength [6]. Many polymers can have their physical, mechanical, and tribological characteristics improved by incorporating

various types of particles and fillers under different loading conditions [7]. Adding TiO_2 nanoparticles to PP/BF composites slightly improved mechanical strength. The composite with 0.4 wt% TiO_2 nanoparticles showed a 5.74% increase in tensile strength and a 4.47% increase in impact strength compared to the untreated composite [8]. In a pultruded composite with epoxy, glass fibers, and modifications using graphene nanoplatelets, aluminum trihydrate, and multi-walled carbon nanotubes, the hybrid nanocomposites showed reduced water absorption and diffusion. This is attributed to the enhanced barrier properties of the hybrid fillers compared to the untreated specimen, owing to the inherent polar nature of epoxy [9]. Particle size significantly affects impact response, with the 4 wt% Nano filler in Epoxy GFRP outperforming all other samples. In Glass Reinforced Epoxy (GRE), incorporating Multi-wall carbon nanotubes (MWCNT) and Silica (SiO_2) nanoparticles at various weight ratios revealed that GRE achieved its highest ultimate strength with 0.1 wt% MWCNT and 1 wt% SiO_2. Similarly, the highest Young's modulus was observed in GRE containing 0.2 wt% MWCNT and 2 wt% SiO_2 [10, 11]. Incorporating filler additives such as $CaCO_3$, Al_2O_3, MgO, and CuO in epoxy-based glass fiber composites substantially enhances tensile, flexural, and impact strength. This improvement, compared to composites with equivalent weight percentages of $CaCO_3$, Al_2O_3, MgO, and TiO_2, is attributed to superior adhesion achieved in composites using CuO, contrasting with those containing TiO_2 [12]. Composites containing nanofillers significantly improve the mechanical, thermal, electrical, and wear properties of the materials when compared to unfilled composites or traditional materials [13, 14]. Adding iron mud boosts erosion resistance in glass fiber–epoxy composites, providing a viable alternative in highly erosive conditions [15]. Glass fiber improves tensile and flexural strengths but adversely affects impact strength in a single mineral filler. Talc introduction in pure PC/ABS enhances tensile strength but diminishes flexural and impact strengths. E-glass fiber/PP composites show enhancements in tensile strength, modulus, bending strength, and modulus compared to bamboo composites [16, 17]. The VARTM technique produced GE composite samples, and hybrid fillers enhanced erosion wear resistance. Composites with hybrid powder fillers outperformed unaltered and single-filler composites [18]. Hybrid composites with areca sheath, jute, and glass demonstrated superior tensile, flexural, compression, impact, and shear properties compared to those made solely from jute fibers and glass fabrics [19]. GF Composites containing 3% wt. nano clay and 3% wt. fly ash as fillers demonstrated superior tensile and impact strength when compared to unfilled glass fiber reinforced epoxy composites [20]. Particulate-filled hybrid composites highlight significant variations in fiber-matrix interfacial bonding, affecting stress concentrations. G-E hybrid composites, incorporating SiC particles, notably enhance tensile and flexural properties [21]. Tensile strength is influenced by fiber concentration, length, and bonding. Increasing fiber content and particulate loading enhance tensile strength, while impact tests indicate higher impact strength with increased fiber content [22]. Incorporating Nano fillers successfully reduces composite laminate brittleness. Extensive experimental research aims to enhance various attributes. SiO_2-modified epoxy composites outperform Al_2O_3 and TiO_2 fillers, demonstrating superior ILSS, flexural strength, and flexural modulus. Alumina modification in epoxy composites increases hardness and enhances impact energy compared to other modifiers [23, 24]. As SiC filler content increases to 10-15 wt.%, mechanical properties (hardness, tensile strength, interlaminar shear strength, flexural strength, impact strength) consistently improve but decline beyond 15 wt.% [25]. Composites with 10% volume of Mg $(OH)_2$ reach the highest ultimate strength at 375.36 MPa, surpassing others. Al_2O_3-filled composites outperform those with fly ash and hematite; however, increasing Al_2O_3, Mg $(OH)_2$, and fly ash in composites leads to a decline in ultimate tensile strength [26]. Adding tungsten carbide powders improves erosion resistance in G-E composites. Analysis of impingement angles shows a brittle erosive wear pattern across all composites, with the highest erosion rate at a 90-degree angle [27].

After reviewing the existing literature, we have initiated the development of innovative composites comprising epoxy, glass fiber, MgO, and TiO_2. These are compared to composites with only epoxy and glass fiber. Our study aims to investigate filler effects on glass fiber-reinforced epoxy composites, focusing on various mechanical properties. Additionally, we seek to establish a correlation between structures and properties through SEM analysis. This research will provide insights into dispersion techniques and hybrid filler effects. The anticipated results are expected to contribute significantly to improving various industry-relevant mechanical processes.

2. Materials and Methods

2.1. Materials

The study utilized Araldite LY 556 resin, which is a medium viscosity, unaltered liquid epoxy resin derived from bisphenol-A. It exhibits a viscosity range of 10,000 to 12,000 mPa.s and a density between 1.15 and 1.20 g/cc at 25°C. This resin was combined with Aradur HY 951, an unmodified aliphatic polyamine characterized by low viscosity (ranging from 10 to 20 mPa.s) and a density between 0.97 and 0.99 g/cc at 25°C, at a weight ratio of 10:1. For the reinforcement material, 13 mil E-glass fabric in a bidirectional mat configuration with a grammage of 430 GSM was employed. This fabric was procured from Shrinath Adhesive Products Pvt. Ltd. in Ahmedabad, India. In order to improve the characteristics of a composite

material, nanoparticles such as Magnesium Oxide and Titanium dioxide are utilized, each possessing the following distinctive properties.

MgO nanoparticles possess an impressive level of purity at 99.95%. They exhibit an average particle size ranging from 30 to 50 nm, with a specific surface area spanning from 20 to 50 m²/g and a true density of 3.58 g/cc. These nanoparticles are known for their remarkable white polyhedral structure. They possess a molar mass of 40.3044 g/mol and have a melting point at a high temperature of 2852°C.

Titanium dioxide (TiO₂) nanoparticles are renowned for their remarkable purity, which reaches an impressive 99.95%. These nanoparticles exhibit an average particle size ranging from 30 to 50 nanometers (nm) and possess a specific surface area spanning from 200 to 220 square meters per gram (m²/g). They also have a true density of 4.23 grams per cubic centimeter (g/cc). With a molar mass of 79.866 grams per mole (g/mol) and a high melting point of 1843°C, these nanoparticles are characterized by their distinctive white spherical structure.

2.2. Fabrication of Epoxy Nanofibers Mixtures

In this study, we employed unsaturated epoxy resin (LY556) as the matrix material (depicted in Figure. 1), along with woven glass fiber fabrics and select fillers for reinforcement. Araldite epoxy hardener (HY951) was utilized as a curing agent and catalyst. To tailor the matrix properties, commercially sourced MgO and TiO₂ particles were incorporated as filler materials.
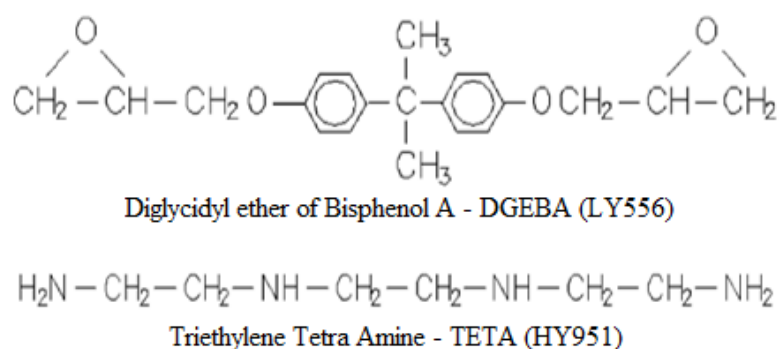

Diglycidyl ether of Bisphenol A - DGEBA (LY556)

Triethylene Tetra Amine - TETA (HY951)

Figure 1. Chemical composition of epoxy compound LY956 and resin HY951 [28]

a. E Glass Fiber preparation   b. Matrix preparation   c. Fiber layers arrangement   d. Vacuum bagging

e. Laminate preparation   f. Laminate machining   g. Specimen preparation   h. Tested specimens

Figure 2. Procedure for creating composite samples

Table 1. Fabrication parameters and levels

Symbol	Process parameters	Levels		
		1	2	3
F.S.S	Fiber stacking sequence	[0/-45/60]$_S$	[0/60/-45]$_S$	[0/45/-45]$_S$
N.F	Nanofillers (MgO+TiO$_2$) wt(%)	0.7	1.2	1.7

Composites Fabrication: At present, the vacuum bagging technique is employed for the production of nine unique epoxy-based fiber-reinforced plastic (FRP) composites (as depicted in Figure. 2), each integrating varying weight proportions of fillers. The process starts with the cutting of fiber mats into pieces measuring 370×330 mm², and each laminate consists of six fiber layers. Following that, a matrix is formed by blending unsaturated epoxy resin (LY556) and hardener Araldite (HY951) in a 10:1 ratio, while maintaining a 50:50 weight ratio between the matrix and fibers. Additionally, powdered filler material is introduced into the mixture at intervals, with precise weight percentages guided by Table 1-3.

To achieve the desired level of consistency, the mixture is stirred using a magnetic stirrer for a duration of 10 to 15 minutes. Take two large, pristine glass molds that exceed the dimensions of the laminate to serve as a base. Securely position a vacuum bagging film over these molds using tape. Layer the fabric sheets atop one another while applying the mixed matrix according to the stacking sequence detailed in Table 1. Include a peel ply for effortless removal post-curing, along with a perforated sheet for resin absorption and a breather sheet. Cover the entire assembly with a bagging sheet, sealing it tightly along the edges with tape. Activate a vacuum pump to eliminate air and excess resin. It's imperative to wait until a stable pressure is achieved to ensure there are no voids in the laminate, resulting in a higher-quality final product.

2.3 Testing Methods of Specimens

2.3.1 Tensile Testing

Tensile testing is carried out in accordance with the ASTM D638 standard [17] and involves the creation of a composite specimen sized at 250 mm × 20 mm × 3 mm. The test is executed utilizing a UTN-40SR double-column universal testing machine, which maintains a constant speed of 1 mm/min within a controlled testing environment. During the testing process, both tensile strain and stress values are automatically logged, and the average ultimate tensile strength (U.T.S) for each trial is included in Table 2. Additionally, the test produces Stress vs. Strain curves, while Figure 3 depicts the load vs. displacement curves, each representing the highest ultimate tensile strength observed from various fiber stacking sequences.

2.3.2 Flexural Testing

The 3-point flexural test is carried out in strict adherence to the ASTM D790 standard [4] procedure, utilizing the MCS computerized UTM2.5-213-0816. Specimens, sized at 125 mm × 12.7 mm × 3 mm, are meticulously prepared and exposed to loading at all specified points as recommended. The testing process is conducted at a controlled cross-head speed of approximately 0.6 mm/min. The fracture load is diligently documented (average F.S displayed in Table 2), and automated generation of strain vs. stress curves is an integral part of the procedure.

2.3.3 Impact Testing

In this experimental assessment, IZOD angles were quantified utilizing a specialized machine designed for evaluating the impact strength of the composite material. The machine employed belongs to the Pendulum Impact type, and the test specimens, with dimensions measuring 64 × 12.7 × 3.3 mm³, were meticulously prepared in accordance with the ASTM D256 standard [17]. The absorbed capacity values are extracted from the Izod Impact Energy Table and subsequently transformed into impact strength (with the average impact strength detailed in Table 2).

2.3.3 Shore D Hardness Test

Following the guidelines outlined in ASTM D2240, the Shore Hardness D method, more commonly referred to as the Durometer hardness test was utilized to evaluate the hardness of composite samples. The specific Durometer used for this assessment is identified as Model TESA 17773. The average results obtained from the testing process are displayed in Table 2. Hardness is determined by measuring the depth of penetration of a durometer indenter foot into the sample under a standardized spring force, and the durometer scale yields a direct reading of the hardness value. To ascertain the enhancement in the mechanical properties of a composite material, initial specimens are fabricated with identical fiber stacking sequences and fiber volume fractions, excluding the addition of nanofillers. The fabrication method and testing procedures for these samples remain consistent. For each specific parameter within every stacking sequence, three samples are prepared, and the highest recorded value is utilized for comparison against samples prepared with the inclusion of nanofillers (MgO+TiO$_2$).
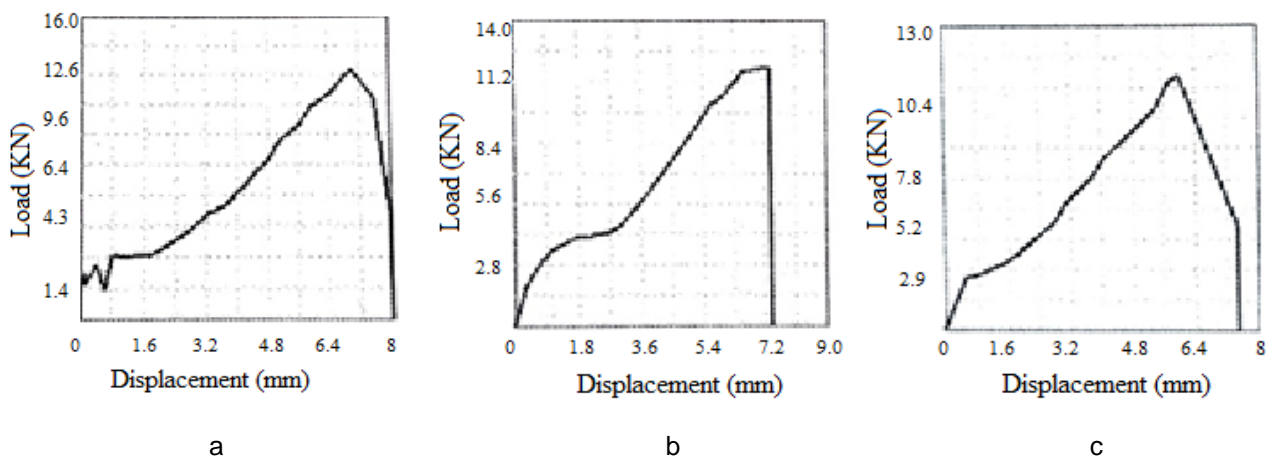
a   b   c

Figure 3. Load Vs Displacement diagrams

Table 2. Taguchi orthogonal array (L9) to represent parameters along with their respective levels and Experimental results

Exp. No.	Parameters				Experimental Results			
	F.S.S	N.F	F.S.S	N.F	U.T.S (MPa)	F.S (MPa)	I.S (J)	H (HV)
1	1	1	[0/-45/60]s	0.7	211.6	138.1	2	72
2	1	2	[0/-45/60]s	1.2	218.7	139.7	4	74
3	1	3	[0/-45/60]s	1.7	235.0	110.3	2.67	71
4	2	1	[0/60/-45]s	0.7	198.3	100.3	2.67	75
5	2	2	[0/60/-45]s	1.2	175.6	105.4	2	70
6	2	3	[0/60/-45]s	1.7	172.2	104.0	2.67	71
7	3	1	[0/45/-45]s	0.7	199.5	105.1	2.67	74
8	3	2	[0/45/-45]s	1.2	176.1	89.4	2	72
9	3	3	[0/45/-45]s	1.7	211.1	107.9	2.67	72

Table 3. Contrasting outcomes when incorporating nanofillers versus excluding them

F.S.S	Experimental Results without nanofillers				Experimental Results with nanofillers				%Improvement			
	U.T.S (MPa)	F.S (MPa)	I.S (J)	H (HV)	U.T.S (MPa)	F.S (MPa)	I.S (J)	H (HV)	U.T.S	F.S	I.S	H
[0/-45/60]s	178	83	4	74	235	139.7	4	74	31.96	68.43	0	0
[0/60/-45]s	193	108	2	74	198	105.4	2.67	75	2.59	-2.41	33.5	1.35
[0/45/-45]s	173	70	2	73	211	107.9	2.67	74	21.97	54.14	33.5	1.37

Table 3 provides a visual representation of the percentage increase or decrease in ultimate tensile strength (U.T.S), flexural strength (F.S), impact strength (I.S), and hardness (H) when evaluated in relation to one another. Upon examination of Table 3, it becomes apparent that in all three fiber stacking sequences, the ultimate tensile strength (U.T.S) experiences an increase, with the highest improvement of 31.96% observed in the [0/-45/60]S sequence. In the case of flexural strength (F.S), a decline is noted in F.S.S2, while it displays significant improvement in the other two stacking sequences (68.43% and 54.14%). When

assessing impact strength (I.S), enhancements are observed in all stacking sequences, except for F.S.S1, where no change is noted. Similarly, in terms of hardness, an increase is observed in F.S.S3 and F.S.S2, while it remains unchanged in F.S.S1.

3. Result and Discussions

3.1 Experimental Results

Table 2 outlines our experimental setup using the Taguchi L9 orthogonal array and summarizes the results, including signal-to-noise (S/N) ratios. Notable findings include:

3.1.1. Tensile Strength

In Experiment 3, the maximum tensile strength of 235.0 MPa was attained by employing a resin-to-hardener ratio of 10:1, [0/-45/60]$_S$ fiber stacking, and incorporating 1.7% nanofillers. In contrast, Experiment 6, conducted under similar conditions and utilizing [0/60/-45]$_S$ fiber stacking, yielded the lowest tensile strength of 172.2 MPa.

3.1.2. Flexural Strength

In Experiment 2, the peak flexural strength of 139.7 MPa was attained by utilizing a resin-to-hardener ratio of 10:1, [0/-45/60]$_S$ fiber stacking, and incorporating 1.2% nanofillers. Conversely, Experiment 8, conducted under similar conditions and employing [0/45/-45]$_S$ fiber stacking, exhibited the lowest flexural strength at 89.4 MPa.

3.1.3. Impact Strength

Experiment 2 exhibited the highest impact strength at 4 J, achieved through a resin-to-hardener ratio of 10:1, [0/-45/60]$_S$ fiber stacking, and the incorporation of 0.7% nanofillers. In contrast, Experiments 1, 5, and 8 displayed lower impact strengths of 2 J under similar conditions, with respective fiber stacking sequences of [0/-45/60]$_S$, [0/60/-45]$_S$, and [0/45/-45]$_S$, and nanofiller contents of 0.7%, 1.2%, and 1.2%.

3.1.4. Vickers Hardness

In Experiment 4, the peak Vickers hardness value of 75 was reached by employing a resin-to-hardener ratio of 10:1, [0/60/-45]$_S$ fiber stacking, and incorporating 0.7% nanofillers. Experiment 5, conducted under identical conditions, yielded a slightly lower Vickers hardness value of 70. However, in this case, the only variation was the nanofiller content, which was increased to 1.2%, and the fiber stacking sequence remained [0/60/-45]$_S$.

These findings provide valuable insights into the material properties and the impact of various factors on them in the experimental setup.

3.2 Taguchi's Approach

The Taguchi method employs a specialized orthogonal array design to efficiently explore the entire parameter space while conducting a limited number of experiments. These experimental outcomes are then transformed to a signal-to-noise ratio. Taguchi advocates for utilizing the S/N ratio as a metric to assess characteristics that deviate from the desired values. The S/N ratio is calculated for each level of process parameters using S/N analysis. In this particular experiment, two factors were selected, namely fiber stacking sequence and nanofillers (wt%), and each factor had three levels. In the experiment, an L9 (3^2) orthogonal array was utilized, and it is illustrated in Table 2. This research aims to maximize tensile strength, flexural strength, impact strength, and hardness. Consequently, a larger the better signal-to-noise (S/N) ratio is deemed advantageous in this study. Equation (1) is utilized for the calculation of S/N ratio attributes [29].

$$\text{LB } \frac{S}{N} \text{ ratio} = (-10) * \log_{10}\left(\frac{1}{n}\right)\sum_{i=1}^{n}\frac{1}{y_i^2} \qquad (1)$$

Where:

'n' is the number of observations or experimental runs and 'y_i' is the response for each observation.

3.3 Influence of Process Parameters on Composite Characteristics

Figure 4 displays main effect plots pertaining to the mechanical properties of composites, specifically Ultimate Tensile Strength (U.T.S), Flexural Strength (F.S), Impact Strength (I.S), and Vickers Hardness (H.V). In Figure 4(a), it becomes evident that substantial enhancement in this property is observed when employing a fiber stacking sequence of 1 [0/-45/60]S along with approximately 1.7% by weight of nanofillers. This combination yields the highest average ultimate tensile strength. In Figure 4(b), it is illustrated that the highest mean flexural strength is achieved with a fiber stacking sequence of 1 ([0/-45/60]$_S$) and a composition of 0.7% MgO+TiO$_2$, emphasizing the optimal parameters. Moving to Figure 4(c), the highest average impact strength is attained by utilizing the optimal parameters, which consist of a fiber stacking sequence of 1 ([0/-45/60]$_S$) and 1.7% of MgO+TiO$_2$. However, with regard to Vickers hardness, as shown in Figure 4(d), the highest mean hardness value is reached by utilizing a combination of parameters that include a fiber stacking sequence of 3 ([0/45/-45]$_S$) and a nanofillers weight percentage of 0.7.

3.4 Determining Optimal Conditions for Response Variables

After completing the tests on the nine specimens, the S/N ratios were computed and incorporated into Table 4.
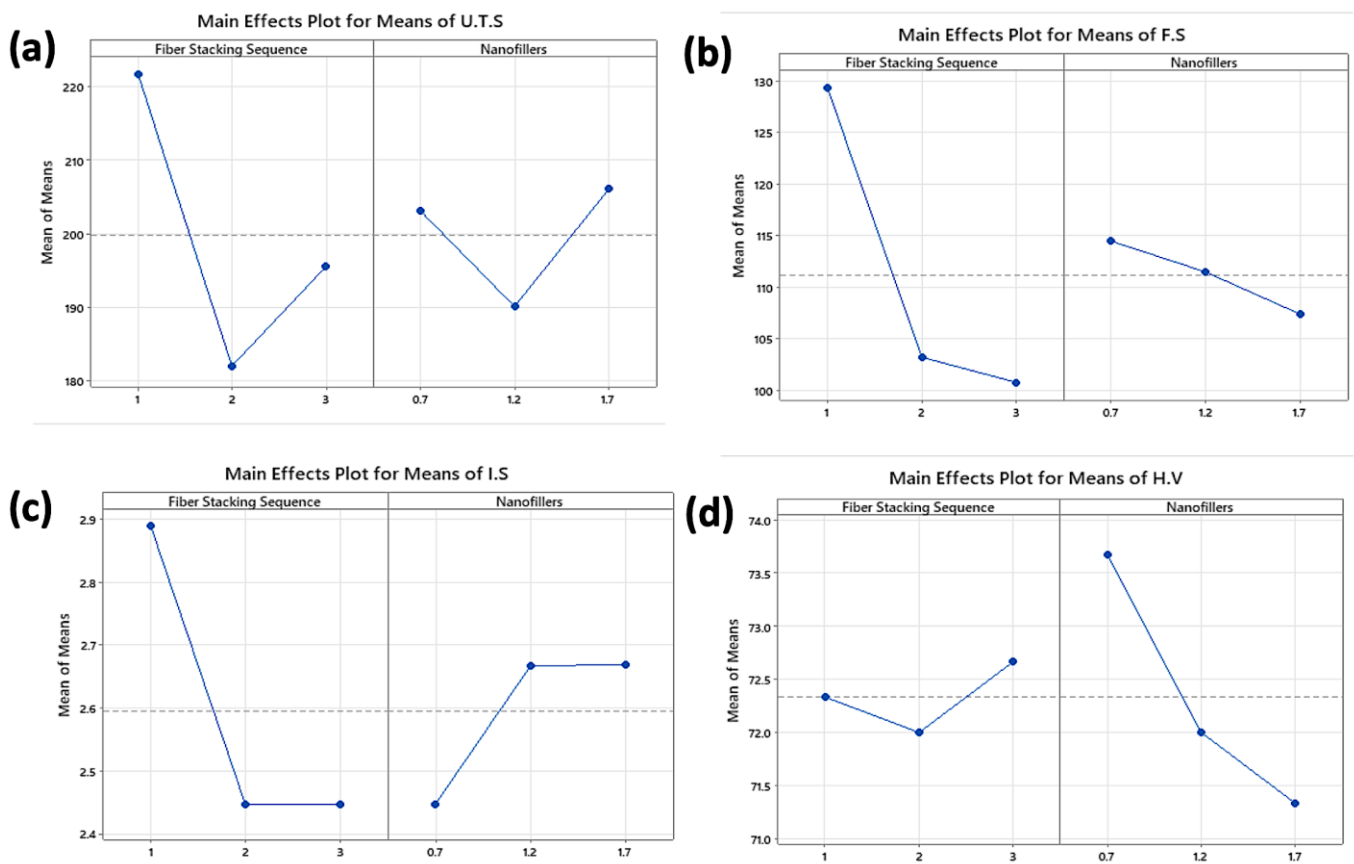
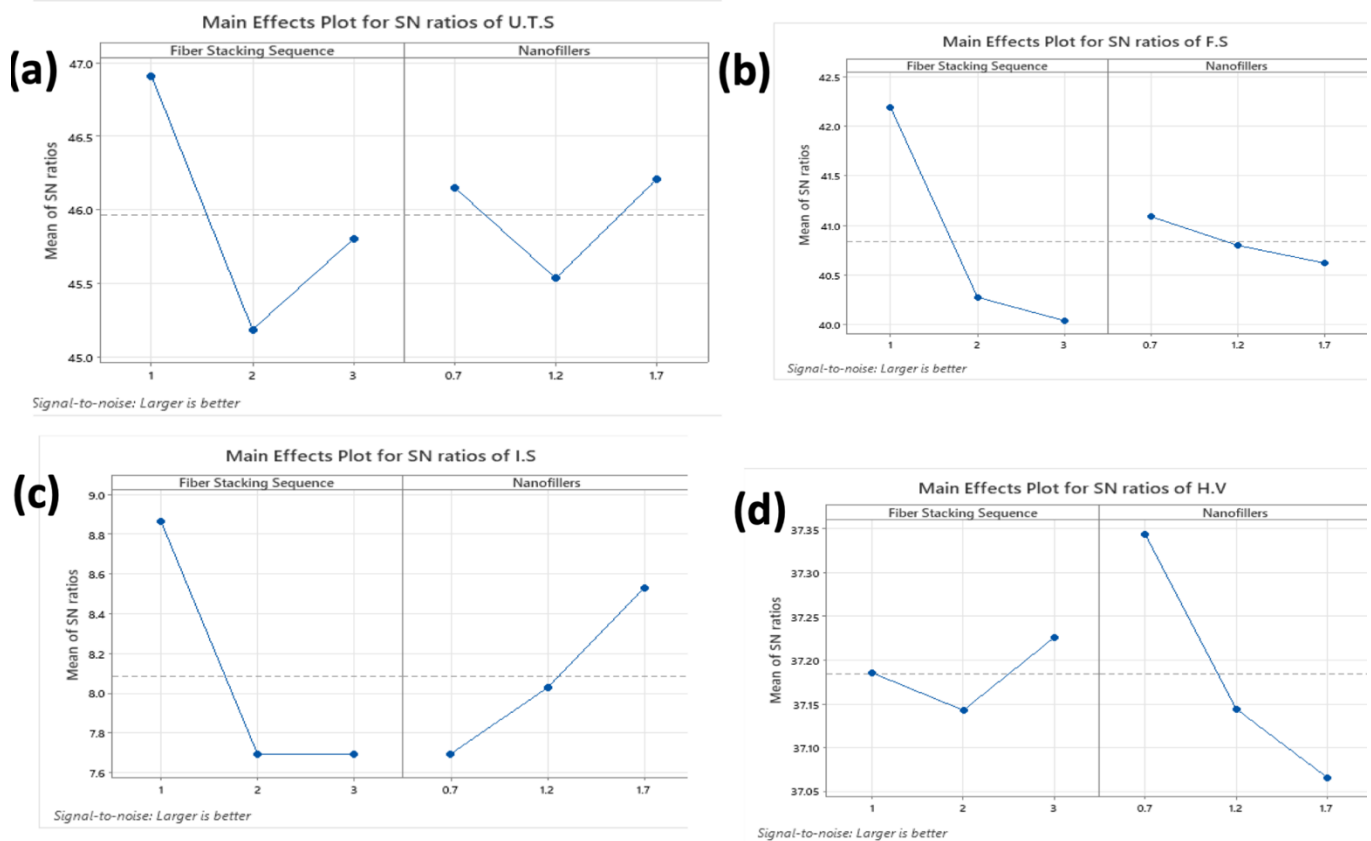**Figure 4.** Main effect plots for means of responses (U.T.S, F.S, I.S, and H.V)

Figure 5. Main effect plots for SN ratios of responses (U.T.S, F.S, I.S, and H.V)

Table 4. Average SN ratio response table for U.T.S

Level	F.S.S	Nanofillers
1	**46.91**	46.15
2	45.19	45.53
3	45.80	**46.21**
Delta	1.72	0.68
Rank	1	2

(a)

Level	F.S.S	Nanofillers
1	**42.19**	**41.09**
2	40.27	40.80
3	40.04	40.62
Delta	2.15	0.47
Rank	1	2

(b)

Level	F.S.S	Nanofillers
1	**8.864**	7.694
2	7.694	8.027
3	7.694	**8.530**
Delta	1.170	0.837
Rank	1	2

(c)

Level	F.S.S	Nanofillers
1	37.19	**37.34**
2	37.14	37.14
3	**37.23**	37.07
Delta	0.08	0.28
Rank	2	1

(d)

It was determined that experiment No.3 displays the highest tensile strength, denoting the parameter set with an F.S.S1N.F3 level equivalent to [0/-45/60]$_S$ fiber orientation and 1.7% of MgO+TiO$_2$ nanomaterial as filler, maintaining a 50:50 ratio of fiber to matrix. In contrast, experiment No. 2 exhibits the maximum flexural strength corresponding to N.S.S1N.F2, characterized by ([0/-45/60]S fiber orientation and 1.2% of MgO+TiO$_2$ Nano filler) with the same fiber volume fraction. The highest impact strength coincides with the flexural strength level, and the highest hardness is observed at F.S.S2N.F1, specifically [0/60/-45] S fiber orientation and 0.7% of MgO+TiO$_2$ nanofiller. The optimal parameter combinations were predicted by estimating different parameter levels and are listed in Table 4. Figure 5 illustrates the distributions of the mean S/N ratios.

3.5 Confirmation Test

To verify the optimal conditions predicted by Taguchi, it is imperative to conduct confirmation tests. These tests utilize the predicted signal-to-noise ratio to assess and validate the anticipated response when operating under the predicted optimal conditions. The calculation of the S/N ratio is based on Equation (2).

$$\varepsilon_{predicted} = \varepsilon_t + \sum_{i=1}^{k}(\varepsilon_m - \varepsilon_t) \qquad (2)$$

Where ε_t = Total mean SN ratio

ε_m = S/N ratio at optimal level.

k = Number of input process parameters.

Under the Taguchi-predicted optimal conditions (Table 4), conformation experiments were conducted, and the outcomes are presented in Table 5 (a-d) for U.T.S, F.S, I.S, and H. The predicted optimal conditions for U.T.S, F.S, I.S, and H demonstrate an enhancement in the performance characteristic results. The signal-to-noise (S/N) ratio enhancements observed under optimal conditions for U.T.S, F.S, I.S, and H were 37.0664, 37.3449, 37.0664, and 37.3854 dB, respectively, in contrast to the initial parameter settings as depicted in Table 5. Based on the validation results, it was determined that the Taguchi-predicted optimal settings yield more favorable outcomes when compared to the initial parameter configurations. In the context of the Taguchi-predicted optimal settings, the improvements in U.T.S, F.S, I.S, and H were measured at 22.08%, 22.35%, 46.36%, and 4.244%, respectively, when contrasted with the initial parameter conditions.

3.6 Analysis of Variance for Response Variables

ANOVA serves the dual purpose of assessing the significance and quantifying the percentage of influence that parameters have on response variables, all the while determining the suitability of the experimental data for further analysis. The ANOVA analysis was conducted with a confidence level of 95% [30], and the outcomes are detailed for the fiber stacking sequence and the weight percentage (wt%) of nanofillers, as presented in Table 6. Significance is inferred from a p-value equal to or less than 0.05. The information provided in Table 6 unquestionably demonstrates the significant influence of both the fiber stacking sequence and nanofillers on the ultimate tensile strength, flexural strength, and impact strength of the composite materials. Specifically, the fiber stacking sequence plays a significant role, contributing to 63.65% of the ultimate tensile strength, 65.70% of the flexural strength, and 9.30% of the impact strength. In contrast, nanofillers have a somewhat lesser influence,

contributing 11.71% to ultimate tensile strength, 2.66% to flexural strength, and 3.61% to impact strength.

Furthermore, when we consider the hardness of the composites, it becomes evident that nanofillers play a more substantial role than the fiber stacking sequence. Nanofillers contribute to 39.22% of the hardness, while the fiber stacking sequence's contribution is notably lower at 3.29%.

The ANOVA results' dependability and adequacy were assessed through the examination of residual (error) plots, as depicted in Figure 6.

Table 5. Conformation test results of U.T.S, F.S, I.S, and H

	Optimum Parameter	
	Initial	Predicted
Level	F.S.S2-N.F2	F.S.S1-N.F3
U.T.S	175.6	214.4
S/N ratio	44.8905	37.0664
Diff. in S/N ratio	7.8241	
%age improved in U.T.S	22.08	

(a)

	Optimum Parameter	
	Initial	Predicted
Level	F.S.S2-N.F2	F.S.S1-N.F1
F.S	105.4	128.95
S/N ratio	40.4568	37.3449
Diff. in S/N ratio	3.1119	
%age improved in F.S	22.35	

(b)

	Optimum Parameter	
	Initial	Predicted
Level	F.S.S2-N.F2	F.S.S1-N.F3
I.S	2	2.9271
S/N ratio	6.0206	37.0664
Diff. in S/N ratio	31.0458	
%age improved in I.S	46.36	

(c)

	Optimum Parameter	
	Initial	Predicted
Level	F.S.S2-N.F2	F.S.S3-N.F1
H	70	72.971
S/N ratio	36.9020	37.3854
Diff. in S/N ratio	0.4834	
%age improved in H	4.244	

(d)

Table 6. Analysis of Variance (ANOVA) for assessing individual quality responses

|	Source	DF	Adj SS	Adj MS	F	P	% Contribution
U.T.S	Fiber Stacking Sequence	2	4.5781	2.2890	5.17	0.078	63.65
	Nanofillers	2	0.8424	0.4212	0.95	0.459	11.71
	Residual Error	4	1.7719	0.4430			
	Total	8	7.1924				
F.S	Fiber Stacking Sequence	2	8.3189	4.1595	4.15	0.106	65.70
	Nanofillers	2	0.3374	0.1687	0.17	0.851	2.66
	Residual Error	4	4.0053	1.0013			
	Total	8	12.6616				
I.S	Fiber Stacking Sequence	2	2.739	1.3697	0.21	0.816	9.30
	Nanofillers	2	1.064	0.5320	0.08	0.922	3.61
	Residual Error	4	25.625	6.4061			
	Total	8	29.428				
HV	Fiber Stacking Sequence	2	0.01038	0.005192	0.11	0.895	3.29
	Nanofillers	2	0.12367	0.061836	1.36	0.353	39.22
	Residual Error	4	0.18127	0.045317			
	Total	8	0.31532				
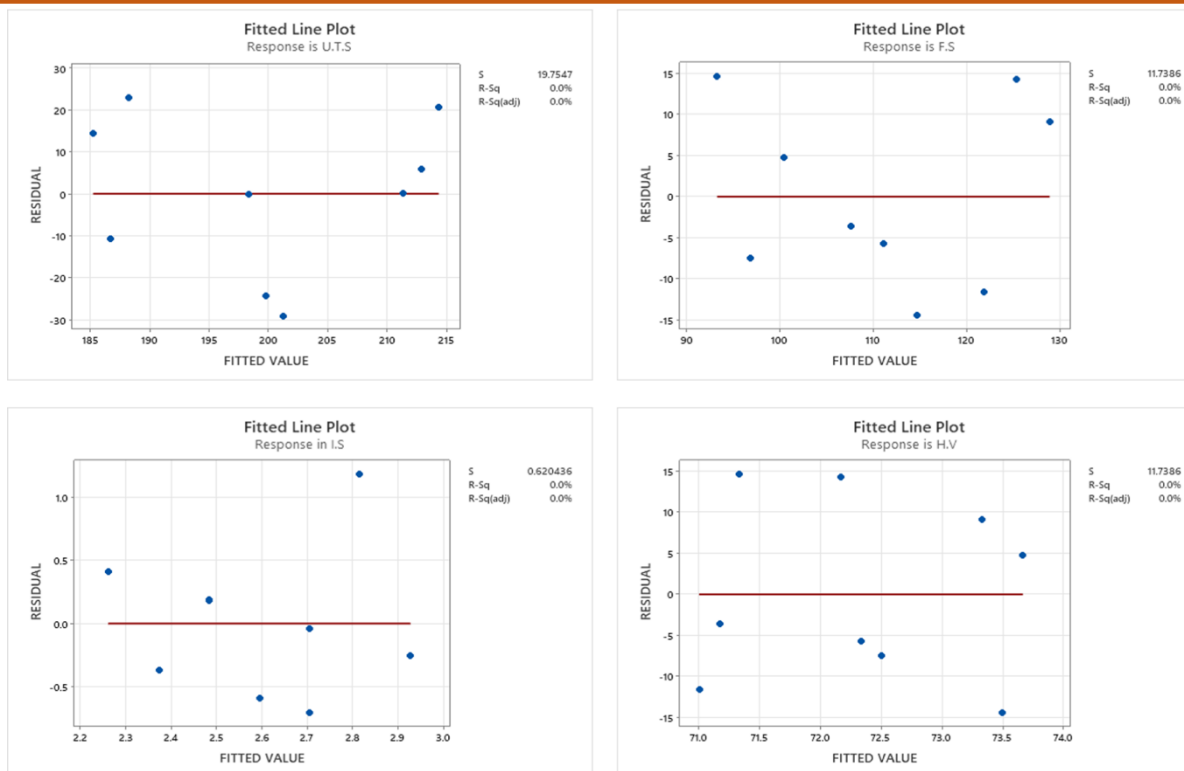
Figure 6. Fitted line plots for responses U.T.S, F.S, I.S, and H.V

These plots provide a visual representation of the relationship between residual and fitted values, enabling efficient verification of the assumptions. In the context of Figure 6, the fitted line plots serve a dual purpose. First and foremost, they provide empirical confirmation of the constancy of variance assumption, illustrating a random distribution of data points on either side of the regression line. This, in turn, validates the critical assumption of constant variance. Beyond this, the amalgamation of these fitted line plots with normality plots and the careful fulfillment of underlying assumptions collectively underpins the assertion that the dataset is well-suited for modeling through a linear regression framework. In this way, the analysis leverages these graphical tools to affirm the model's appropriateness for the given dataset.

3.7 Modelling

In the current investigation, we employed linear regression analysis utilizing the Minitab 20 software to construct predictive mathematical models for the dependent variables, namely U.T.S, F.S, I.S, and H. These models were developed in relation to the factors of fiber stacking sequence and nanofillers ($MgO+TiO_2$), and no data transformations were applied to the responses. The resulting predictive equations derived from the regression analysis are denoted as Eqn. (3) for U.T.S, Eqn. (4) for F.S, Eqn. (5) for I.S, and Eqn. (6) for H, respectively.

U.T.S = 222.4 - 13.10 Fiber Stacking Sequence + 3.0 Nanofillers   (3)

F.S = 148.2 - 14.28 Fiber Stacking Sequence - 7.1 Nanofillers   (4)

I.S = 2.770 - 0.222 Fiber Stacking Sequence + 0.223 Nanofillers   (5)

HV = 74.80 + 0.167 Fiber Stacking Sequence - 2.33 Nanofillers   (6)

If the residual chart displays a linear pattern, it indicates that the residual errors within the model follow a normal distribution, and the coefficients in the model hold significance. The residual plots for U.T.S, F.S, I.S, and H can be observed in Figure 7. Examination of Figure 7 reveals that the residuals closely align with the linear trend for all the response variables, indicating the significance of the developed model.

3.8 Scanning Electron Microscope Analysis

SEM analysis was performed using a JEOL instrument with model number JSM-5300LV, operating at a voltage acceleration of 10 kV. Tensile samples were inspected for each design, and Figure 8 (a-c) displays the cross-sectional area, revealing the structural characteristics of the composites.

SEM analysis was carried out on the composites to visually assess material morphology, evaluate the effectiveness of filler material dispersion (uniform distribution), and determine the continuity of glass fibers. Noticeable distinctions in the internal structure and filler distribution within the sample volume were observed among the prepared composites.
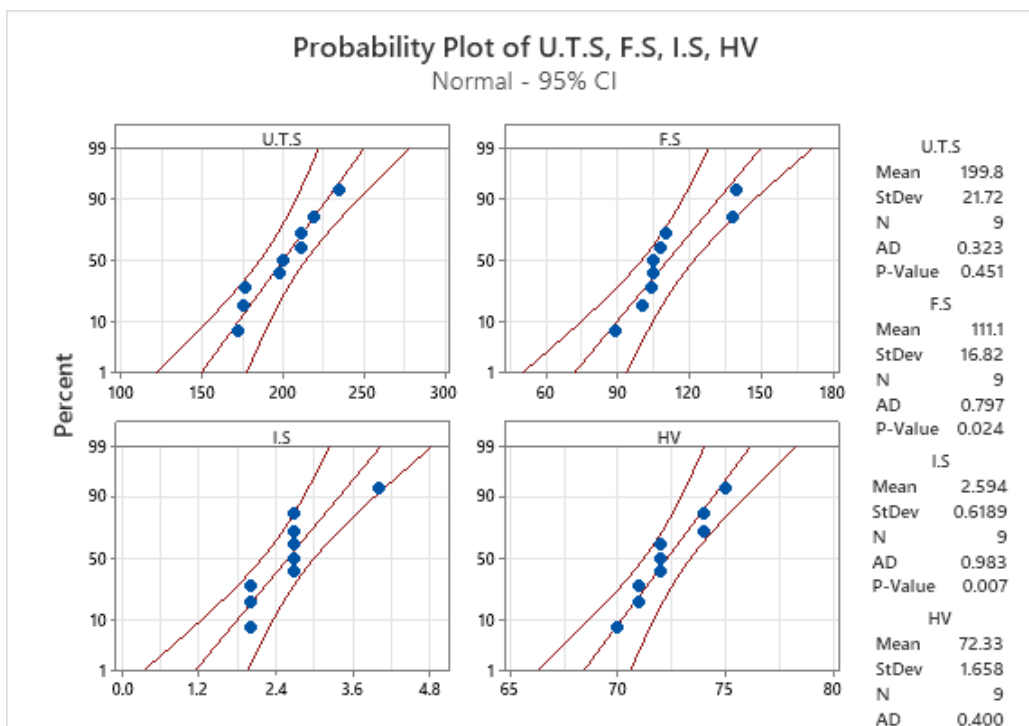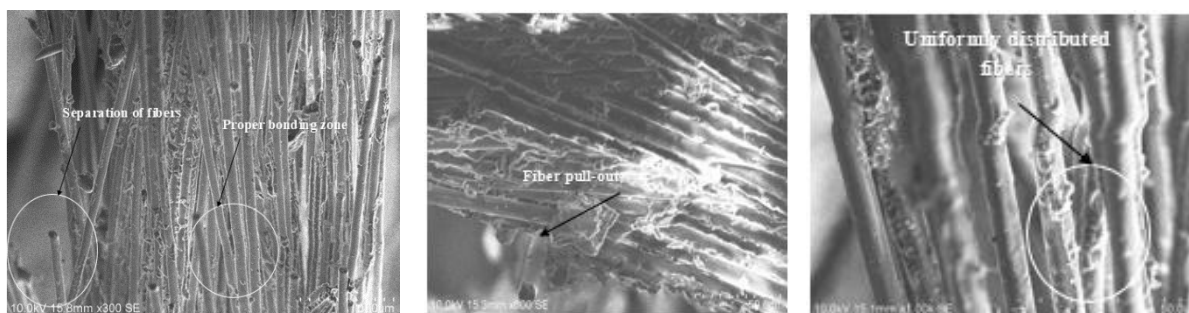
Figure 7. Normal probability plots for responses U.T.S, F.S, I.S, and H.V

(a)1.3 T1 ([0/-45/60]S @1.7%)   (b) 2.1 T5 ([0/60/-45]s, @ 0.7%)   (c) 3.3 T2 ([0/45/-45]S) @1.7%)

Figure 8. SEM images of the cross-sectional area of specimen ID a) 1.3 b) 2.1 c) 3.3

The specimens, as illustrated in Figure 8, exhibited uniform and continuous glass fiber distribution throughout the sample volume. Significant alterations in the material's microstructure were observed after modification with MgO and TiO$_2$. Based on the observations from Figure 8 (a-c), it is clear that specimens 1.3 and 3.3 demonstrate strong adhesion among the matrix, fillers, and fibers, in stark contrast to specimen 2.2. Consequently, these specimens exhibit enhanced mechanical properties. The lack of adhesion between the glass fiber laminate and filler materials is conspicuous on the fractured surfaces, signaling inadequate interfacial interaction, which likely contributes to the decrease in mechanical performance. Notably, a positive correlation was found between filler content and interactions. Both blends exhibited satisfactory interfacial adhesion with MgO and TiO$_2$.

4. Conclusion

The following conclusions were derived from the experimental findings:

- A comparison between composite materials with and without nanofillers demonstrated noteworthy improvements in response variables. Specifically, there was a substantial 31.96% increase in ultimate tensile strength and a significant 68.43% enhancement in flexural strength. When these findings are juxtaposed with those from the literature [12], it is evident that the tensile strength increased by approximately 51.41%, while the flexural strength decreased by 34.88%, attributing these changes to the absence of nanofillers other than MgO and TiO$_2$.

- Executing confirmation experiments based on Taguchi-predicted optimal conditions revealed notable performance improvements in U.T.S, F.S, I.S, and H. These ideal conditions resulted in Signal-to-Noise (S/N) ratios of 37.0664, 37.3449, 37.0664, and 37.3854 dB for U.T.S, F.S, I.S, and H, respectively, in contrast to the initial settings.

- Validation results confirmed that the Taguchi-predicted settings outperformed the initial configurations, resulting in improvements of 22.08% for U.T.S, 22.35% for F.S, 46.36% for I.S, and 4.244% for H.

- The ANOVA results reveal that fiber stacking sequence significantly impacts ultimate tensile strength (63.65%), flexural strength (65.70%), and impact strength (9.30%). On the other hand, nanofillers have a lesser influence, contributing 11.71% to ultimate tensile strength, 2.66% to flexural strength, and 3.61% to impact strength. However, when it comes to composite hardness, nanofillers play a more substantial role, contributing 39.22%, while the fiber stacking sequence has a notably lower influence at 3.29%.

- Upon inspecting the normal probability plots, it becomes evident that the residuals closely follow the linear trend for all the response variables, underscoring the significance of the constructed model.

References

[1] R. Sundarakannan, K. Balamurugan, Y. Jyothi, V. Arumugaprabu, T. Sathish, Z. Mahmoud, El S. Yousef, D. Basheer, S. Shaik, Importance of Fiber-/Nanofiller-Based Polymer Composites in Mechanical and Erosion Performance: A Review. Journal of Nanomaterials, 2023, (2023). https://doi.org/10.1155/2023/3528977

[2] G. Lawal, C. Kuforiji, S. Durowaye, K. Kassim, Study of the mechanical properties of bamboo and glass fiber reinforced hybrid polymer matrix composites. Kathmandu University Journal of Science Engineering and Technology, 17(1), (2023) 1-5.

[3] C. Rajesh Chandra, S.K. Jagadeesh, D. Aravinda, H. Jayanth, Mechanical and Three Body Abrasive Wear Behaviour of Nano-Filler Filled, Chopped Glass Fiber Filled Hybrid Composites. International Journal of Scientific Research in Science, Engineering and Technology (IJSRSET), 9(6), (2022) 292-299. https://doi.org/10.32628/IJSRSET229651

[4] A.A. Rajhi, Mechanical Characterization of Hybrid Nano-Filled Glass/Epoxy Composites. Polymers, 14(22), (2022) 4852. https://doi.org/10.3390/polym14224852

[5] M. Ramesh, L.N. Rajeshkumar, N. Srinivasan, D.V. Kumar, & D. Balaji, Influence of filler material on properties of fiber-reinforced polymer composites: A review. E-Polymers, 22(1), (2022) 898-916. https://doi.org/10.1515/epoly-2022-0080

[6] A. Rakhman, K. Diharjo, W.W. Raharjo, V. Suryanti, S. Kaleg, Improvement of Fire Resistance and Mechanical Properties of Glass Fiber Reinforced Plastic (GFRP) Composite Prepared from Combination of Active Nano Filler of Modified Pumice and Commercial Active Fillers. Polymers, 15(1), (2023) 51. https://doi.org/10.3390/polym15010051

[7] H.I. Elkhouly, E.M. Ali, M.N. El-Sheikh, An investigated organic and inorganic reinforcement as an effective economical filler of poly (methyl methacrylate) nanocomposites. Scientific Reports, 12, (2022) 16416. https://doi.org/10.1038/s41598-022-20393-3

[8] J. Guo, M. Cao, W. Ren, H. Wang, & Y. Yu, Mechanical, dynamic mechanical and thermal properties of TiO_2 nanoparticles treatment bamboo fiber-reinforced polypropylene composites. Journal of Materials Science, 56, (2021) 12643–12659. https://doi.org/10.1007/s10853-021-06100-z

[9] R. Balasubramanya, R.R.N.S. Bhattacharya, & B.M. Madhu, Effect of Hybrid Fillers on GFRP Epoxy Composites with Water Immersion and Thermal Conditioning. Macromolecular Symposia, 398(1), (2021) 2000090. https://doi.org/10.1002/masy.202000090

[10] K. Sravanthi, V. Mahesh, B. Nageswara Rao, Influence of micro and nano carbon fillers on impact behavior of GFRP composite materials. Materials Today: Proceedings, 37(2), (2020) 1075-1078. https://doi.org/10.1016/j.matpr.2020.06.298

[11] A.A.F. Ogaili, E.S. Al-Ameen, M.S. Kadhim, & M.N. Mustafa, Evaluation of mechanical and electrical properties of GFRP composite strengthened with hybrid nanomaterial fillers. AIMS Materials Science, 7(1), (2020) 93-102. https://doi.org/10.3934/matersci.2020.1.93

[12] M.S. Alam, & M.A. Chowdhury, Characterization of epoxy composites reinforced with $CaCO_3$-Al_2O_3-MgO-TiO_2/CuO filler materials. Alexandria Engineering Journal, 59(6), (2020) 4121-4137. https://doi.org/10.1016/j.aej.2020.07.017

[13] R. Olayil, V. Arumugaprabu, O. Das, & W.L. Anselm, A Brief Review on Effect of Nano fillers on Performance of Composites. In IOP Conference Series: Materials Science and Engineering, IOP Publishing, 1059,d (2021) 012006. https://doi.org/10.1088/1757-899X/1059/1/012006

[14] I.S. Shayea, J.R. Ugal, Influence of Some Nano-Inorganic Oxides on the Mechanical Properties of Epoxy Based Nano Composites. In IOP Conference Series: Materials Science and Engineering, IOP Publishing, 571, (2019) 012068. https://doi.org/10.1088/1757-899X/571/1/012068

[15] B. Pani, P. Chandrasekhar, S. Singh, Investigation of erosion behaviour of an iron-mud filled glass-fibre epoxy hybrid composite. Bulletin of Materials Science, 42(217), (2019). https://doi.org/10.1007/s12034-019-1894-1

[16] E. Kuram, Hybridization effect of talc/glass fiber as a filler in polycarbonate/acrylonitrile-butadiene-styrene composites. Composites Part B: Engineering, 173, (2019) 106954. https://doi.org/10.1016/j.compositesb.2019.106954

[17] K.N. Keya, N.A. Kona, & R.A. Khan, Fabrication, Mechanical Characterization and Interfacial Properties of Bamboo and E-glass Fiber Reinforced Polypropylene-based Composites. American Journal of Nanosciences, 5(4), (2019) 59-66. https://doi.org/10.11648/j.ajn.20190504.16

[18] P.H. Usha Rani, B.M. Rajaprakash, N. Mohan, & M. Akshay Prasad, Study on thermal and erosive wear behaviour of hard powders filled glass-epoxy composite. Materials Today: Proceedings, 27(3), (2020) 2011-2016. https://doi.org/10.1016/j.matpr.2019.09.049

[19] S. Jothibasu, S. Mohanamurugan, R. Vijay, D. Lenin Singaravelu, A. Vinod, & M.R. Sanjay, Investigation on the mechanical behavior of areca sheath fibers/jute fibers/glass fabrics reinforced hybrid composite for light weight applications. Journal of Industrial Textiles, 49, (2020) 1036-1060. https://doi.org/10.1177/1528083718804207

[20] S. Mutalikdesai, A. Hadapad, S. Patole, & G. Hatti, Fabrication and Mechanical Characterization of Glass fibre reinforced Epoxy Hybrid Composites using Fly ash/Nano clay/Zinc oxide as filler. IOP Conference Series: Materials Science and Engineering, 376, (2018) 012061. https://doi.org/10.1088/1757-899X/376/1/012061

[21] B. Hulugappa, M.V. Achutha, B. Suresha, Effect of Fillers on Mechanical Properties and Fracture Toughness of Glass Fabric Reinforced Epoxy Composites. Journal of Minerals and Materials Characterization and Engineering, 4(1), (2016) 1-14. http://dx.doi.org/10.4236/jmmce.2016.41001

[22] S.S. Moorthy, & K. Manonmani, Statistical Analysis and Predictive Learning of Mechanical Parameters for TiO_2 Filled GFRP Composite. International Journal of Mechanical and Mechatronics Engineering, 8, (2014) 119-123. https://doi.org/10.5281/zenodo.1090713

[23] S. Kumar, S. Raju, N. Mohana, P.S. Sampath, & L.S. Jayakumari, Effects of Nanomaterials on Polymer Composites-An Expatiate View. Reviews on Advanced Materials Science, 38(1), (2014) 40-54.

[24] R.K. Nayak, A. Dash, & B.C. Ray, Effect of Epoxy Modifiers ($Al2O_3$/SiO_2/TiO_2) on Mechanical Performance of epoxy/glass Fiber Hybrid Composites. Procedia Materials Science, 6, (2014) 1359–1364. https://doi.org/10.1016/j.mspro.2014.07.115

[25] G. Agarwal, A. Patnaik, & R. Sharma, Thermo-mechanical properties of silicon carbide filled chopped glass fiber reinforced epoxy composites. International Journal of Advanced Structural Engineering, 5, (2013) 21. https://doi.org/10.1186/2008-6695-5-21

[26] K. Devendra, T. Rangaswamy, Strength Characterization of E-glass Fiber Reinforced Epoxy Composites with Filler Materials. Journal of Minerals and Materials Characterization and Engineering, 1(6), (2013) 353-357. http://dx.doi.org/10.4236/jmmce.2013.16054

[27] N. Mohan, C.R. Mahesha, & B.M. Rajaprakash, Erosive Wear Behaviour of WC Filled Glass Epoxy Composites. Procedia Engineering, 68, (2013) 694–702. https://doi.org/10.1016/j.proeng.2013.12.241

[28] S. Rao, & R. Rao, Cure studies on bifunctional epoxy matrices using a domestic microwave oven. Polymer Testing, 27(5), (2008) 645–652. https://doi.org/10.1016/j.polymertesting.2008.04.005

[29] S.S. Yusuf, M.N. Islam, M.H. Ali, M.W. Akram, M.A. Siddique, Towards the optimization of process parameters for impact strength of natural fiber reinforced composites: Taguchi method, Advances in Materials Science, 20(2), (2020) 54-70. https://doi.org/10.2478/adms-2020-0010

[30] M.I. Qazi, M. Abas, R. Khan, W. Saleem, C.I. Pruncu, & M. Omair, Experimental Investigation and Multi-Response Optimization of Machinability of AA5005H34 Using Composite Desirability Coupled with PCA. Metals, 11(2),

(2021)   235.
https://doi.org/10.3390/met11020235

[31]   P. Sivaiah, & D. Chakradhar, Modeling and optimization of sustainable manufacturing process in the machining of 17-4 PH stainless steel. Measurement, 134, (2018) 142-152. https://doi.org/10.1016/j.measurement.2018.10.067

Authors Contribution Statement

A. Somaiah; Conceptualized and designed the study, data collection, conducted analysis, and original manuscript drafting and coordination. B. Anjaneya Prasad; N. Kishore Nath; Conceptualization, Review, writing and editing. N. Kishore Nath; Conceptualization and design, Review, writing and editing.

Funding sources

Has this article screened for similarity?

Yes

About the License